Supporting Information

Bandgap Engineering of Lead-Free Iron-Based Halide Double Perovskite Single Crystals and Nanocrystals by Alloying or Doping Strategy

Peigeng Han[a,b], Cheng Luo[a,b], Wei Zhou[a], Jie Hou[a,b], Cheng Li[a,c], Daoyuan Zheng[c], and Keli Han[a,c*]

[a] State Key Laboratory of Molecular Reaction Dynamics, Dalian Institute of Chemical Physics, Chinese Academy of Science, Dalian 116023, P. R. China.

[b] University of the Chinese Academy of sciences, Beijing 100049, P. R. China.

[c] Institute of Molecular Sciences and Engineering, Shandong University, Qingdao 266237, P. R. China.

[*]Corresponding author. E-mail: klhan@dicp.ac.cn

This file includes:

Experimental section

Tables S1-S9

Figures S1-S16

Experimental section

Materials.

Cesium chloride (CsCl, 99%, Aladdin), sodium chloride (NaCl, 99.99%, Alfa Aesar), silver chloride (AgCl, 99.9%, Alfa Aesar), iron chloride ($FeCl_3$, 99.9%, anhydrous, Aladdin), bismuth chloride ($BiCl_3$, anhydrous, 99%, Alfa Aesar), antimonous chloride ($SbCl_3$, 99.9%, Alfa Aesar), indium chloride($InCl_3$, 98%, Sigma-Aldrich), hydrochloric acid (analytical pure, Sinopharm Chemical Reagent Co., Ltd, China), n-hexane (97%, Aladdin), toluene (99.5%, Sinopharm Chemical Reagent Co., Ltd, China), isopropanol (High performance liquid chromatography pure, Kermel, China), oleic acid (OA, 90%, Alfa Aesar). All chemicals are used as received without further purification.

Synthesis of $Cs_2Ag_xNa_{1-x}FeCl_6$ ($0 \leq x \leq 1$) single crystals (SCs) by hydrothermal method.

For the $Cs_2Ag_xNa_{1-x}FeCl_6$ (x = 0, 0.01, 0.05, 0.1, 0.25, 0.5, 0.75, and 1) SCs, 2 mmol CsCl, 1 mmol $FeCl_3$, x mmol AgCl and 1-x mmol NaCl are dissolved in 10 mL hydrobromic acid in a 20 mL Teflon liner. Then, it is heated at 180 °C for 16 hours in a stainless steel Parr autoclave, and is slowly cooled to room temperature (RT) at a speed of 5-8 °C/h. Finally, the SCs are filtered and dried in vacuum at 70 °C for 10 h.

Synthesis of $Cs_2M'MCl_6$ (M' = Na, or Ag; M = In, Sb, or Bi) SCs and $Cs_2M'M_{0.9}Fe_{0.1}Cl_6$ (M' = Na, or Ag; M = In, Sb, or Bi) SCs by hydrothermal method.

For $Cs_2M'MCl_6$ (M' = Na, or Ag; M = In, Sb, or Bi) DP SCs, 2 mmol CsCl, 1 mmol M'Cl (M' = Na, or Ag) and 1 mmol MCl_3 (M = In, Sb, or Bi) are dissolved in 10 mL hydrobromic acid in a 20 mL Teflon liner, respectively. Then, it is heated at 180 °C for 16 hours in a stainless steel Parr autoclave, and is slowly cooled to room temperature (RT) at a speed of 5-8 °C/h. Finally, the SCs are filtered and dried in vacuum at 70 °C for 10 h.

For Fe-doped DP SCs, 2 mmol CsCl, 1 mmol M'Cl (M' = Na, or Ag), 0.9 mmol MCl_3 (M = In, Sb, or Bi) and 0.1 mmol $FeCl_3$ are dissolved in 10 mL hydrobromic acid in a 20 mL Teflon liner, respectively. Then, it is heated at 180 °C for 16 hours in a stainless steel Parr autoclave, and is slowly cooled to room temperature (RT) at a speed of 5-8 °C/h. Finally, the SCs are filtered and dried in vacuum at 70 °C for 10 h.

Synthesis of $Cs_2FeCl_5(H_2O)$ SCs by cooling crystallization method.

2 mmol CsCl, and 1 mmol $FeCl_3$ are dissolved in 10 mL hydrobromic acid in a 50 mL flask. Then, it is heated at 110 °C for 4 hours, and is slowly cooled to room temperature (RT) at a speed of 5-8 °C/h. Finally, the SCs are filtered and dried in vacuum at 70 °C for 10 h.

Synthesis of $Cs_2Ag_xNa_{1-x}FeCl_6$ (x = 0, 0.25, 0.5, 0.75, and 1) nanocrystals (NCs) by ultrasonic crushing method.

The SCs are ground into a micron-sized powder. The powder (0.04 g) is added to 10 mL antisolvent (hexane, mixed solution of 80% toluene and 20% isopropanol), which are ultrasonicated by an ultrasonic probe (Scientz-IID, 300 W, ultrasonic homogenizer, Ningbo, China) for 20 min at 60 °C. Then, the solution is centrifuged for 5 min at 1000 rpm/min to discard the large crystals, and the supernatant solution containing the NCs was obtained. After this, the colloidal NCs solution is further centrifuged for 5 min at 5000 rpm/min, we obtain the NCs precipitate for further

characterization.

Structural characterizations.

Powder X-ray diffraction (PXRD) is performed on an PANalytical Empyrean diffractometer equipped with Cu Kα X-ray (λ = 1.54056 Å) tubes, and the acquisition is done for every 0.04° increment. A field emission scanning electron microscope (FESEM, JEOL, JSM-7800F, 3kV) equipped with an Oxford X-Max silicon drift detector is used to record the surface morphology and perform chemical analysis. The transmission electron microscopy (TEM) measurements are performed by using the JEM-2100. Thermogravimetric analysis (TGA) thermogram is operated under a nitrogen atmosphere with a Netzsch STA 449 F3Jupiter thermo-microbalance at a heating rate of 10 °C/min. Inductively coupled plasma optical emission spectrometer （ICP-OES) is performed on PerkinElmer ICP-OES 7300DV. Electron spin resonance (ESR) measurement was done using the Bruker A300 spectrometer operated at X-band frequency at room temperature.

Single crystal X-ray diffraction (SCXRD).

A suitable single crystal was selected. Data collections were performed on a Bruker D8 venture CCD area detector' diffractometer with the use of IμS 3.0 microfocus X-ray Mo Kα radiation (λ = 0.71073 Å). The crystal was kept at 293 K for $Cs_2NaFeCl_6$ and $Cs_2AgFeCl_6$ during data collection. Data reduction, cell refinement and experimental absorption correction were performed with the software package of APEX 3. Using Olex2, the structure was solved with the ShelXT structure solution program using Intrinsic Phasing and refined with the ShelXL refinement package using Least Squares minimisation.

Optical absorption spectroscopy.

For colloidal NCs, steady-state optical absorption measurement is performed by using the PerkinElmer Lambda 35 double-beam spectrometer equipped with integrating sphere to exclude signal due to light scattering.

For single crystal powder, steady-state absorption spectra are recorded using a UV−vis (SHIMADZU UV2600) spectrometer. Optical diffuse reflectance measurements are performed by equipping with an integrating sphere at room temperature and $BaSO_4$ as the 100% reflectance reference. The reflectance data are converted to absorption according to the Kubelka−Munk equation:

$$F(R) = (1-R)^2(2R)^{-1} = \frac{\alpha}{S}$$

where R is the reflectance, α and S are the absorption and scattering coefficients, respectively.

Raman spectroscopy.

The Raman measurements are carried out using an inVia Raman Microscope spectrometer (Renishaw). The single crystals are ground into powder and then mounted on a glass substrate to be measured. The Raman spectra are recorded by 532 nm excitation.

Table S1. SCXRD data of $Cs_2NaFeCl_6$ single crystal.

Empirical formula	$Cl_{12}Cs_4Fe_2Na_2$
Formula weight	1114.72
Temperature/K	293(2)
Crystal system	cubic
Space group	Fm-3m
a/Å	10.3263(2)
b/Å	10.3263(2)
c/Å	10.3263(2)
α/°	90
β/°	90
γ/°	90
Volume/Å^3	1101.12(6)
Z	2
ρ_{calc}g/cm^3	3.362
μ/mm^{-1}	9.312
F(000)	996
Crystal size/mm^3	0.06 × 0.05 × 0.03
Radiation	MoKα (λ = 0.71073)
2Θ range for data collection/°	6.834 to 54.828
Index ranges	$-13 \leq h \leq 13$, $-13 \leq k \leq 13$, $-13 \leq l \leq 13$
Reflections collected	4312
Independent reflections	91 [R_{int} = 0.0251, R_{sigma} = 0.0069]
Data/restraints/parameters	91/0/8
Goodness-of-fit on F^2	1.155
Final R indexes [I>=2σ (I)]	R_1 = 0.0086, wR_2 = 0.0213
Final R indexes [all data]	R_1 = 0.0086, wR_2 = 0.0213
Largest diff. peak/hole / e Å^{-3}	0.27/-0.31

Table S2. SCXRD data of $Cs_2AgFeCl_6$ single crystal.

Empirical formula	$Ag_2Cl_{12}Cs_4Fe_2$
Formula weight	1284.48
Temperature/K	293(2)
Crystal system	cubic
Space group	Fm-3m
a/Å	10.2605(2)
b/Å	10.2605(2)
c/Å	10.2605(2)
α/°	90
β/°	90
γ/°	90
Volume/Å^3	1080.20(6)
Z	2
ρ_{calc}g/cm^3	3.949
μ/mm^{-1}	11.212
F(000)	1140
Crystal size/mm^3	0.11 × 0.08 × 0.04
Radiation	MoKα (λ = 0.71073)
2Θ range for data collection/°	6.878 to 54.706
Index ranges	$-12 \leq h \leq 13$, $-13 \leq k \leq 13$, $-13 \leq l \leq 13$
Reflections collected	4015
Independent reflections	86 [R_{int} = 0.0221, R_{sigma} = 0.0061]
Data/restraints/parameters	86/0/8
Goodness-of-fit on F^2	1.18
Final R indexes [I>=2σ (I)]	R_1 = 0.0119, wR_2 = 0.0267
Final R indexes [all data]	R_1 = 0.0119, wR_2 = 0.0267
Largest diff. peak/hole / e Å^{-3}	0.57/-0.30

Table S3. Summary of the SEM-EDS results.

$Cs_2Ag_xNa_{1-x}FeCl_6$	SEM-EDS results	
	Na (atomic %)	Ag (atomic %)
x = 0.01	98.8	1.2
x = 0.05	94.9	5.1
x = 0.1	91.7	8.3
x = 0.25	74.9	25.1
x = 0.5	50.8	49.2
x = 0.75	24.5	75.5

Table S4. SCXRD data of $Cs_2FeCl_5(H_2O)$ single crystal.

Empirical formula	$Cl_5Cs_2FeH_2O$
Formula weight	516.94
Temperature/K	290
Crystal system	orthorhombic
Space group	Cmcm
a/Å	7.3906(10)
b/Å	17.235(2)
c/Å	8.0201(11)
α/°	90
β/°	90
γ/°	90
Volume/Å^3	1021.6(2)
Z	4
ρ_{calc}g/cm^3	3.361
μ/mm^{-1}	9.740
F(000)	924
Radiation	MoKα (λ = 0.71073)
Index ranges	$-7 \le h \le 10$, $-22 \le k \le 12$, $-10 \le l \le 8$
Goodness-of-fit on F^2	1.061
Final R indexes [I>=2σ (I)]	R_1 = 0.0346, wR_2 = 0.0942
Final R indexes [all data]	R_1 = 0.0346, wR_2 = 0.0942

Table S5. The ICP-OES results of $Cs_2AgSb_{0.9}Fe_{0.1}Cl_6$ SCs.

$Cs_2AgSb_{0.9}Fe_{0.1}Cl_6$		
Fe (mg/L)	Sb (mg/L)	Fe (%)
0.848	11.71	13.64

Table S6. The ICP-OES results of $Cs_2AgBi_{0.9}Fe_{0.1}Cl_6$ SCs.

$Cs_2AgBi_{0.9}Fe_{0.1}Cl_6$		
Fe (mg/L)	Bi (mg/L)	Fe (%)
0.118	38.12	1.15

Table S7. The ICP-OES results of $Cs_2AgIn_{0.9}Fe_{0.1}Cl_6$ SCs.

$Cs_2AgIn_{0.9}Fe_{0.1}Cl_6$		
Fe (mg/L)	In (mg/L)	Fe (%)
0.264	38.72	1.38

Table S8. The ICP-OES results of $Cs_2NaBi_{0.9}Fe_{0.1}Cl_6$ SCs.

$Cs_2NaBi_{0.9}Fe_{0.1}Cl_6$		
Fe (mg/L)	Bi (mg/L)	Fe (%)
0.163	42.34	1.42

Table S9. The ICP-OES results of $Cs_2NaIn_{0.9}Fe_{0.1}Cl_6$ SCs.

$Cs_2NaIn_{0.9}Fe_{0.1}Cl_6$		
Fe (mg/L)	In (mg/L)	Fe (%)
0.153	42.02	0.74

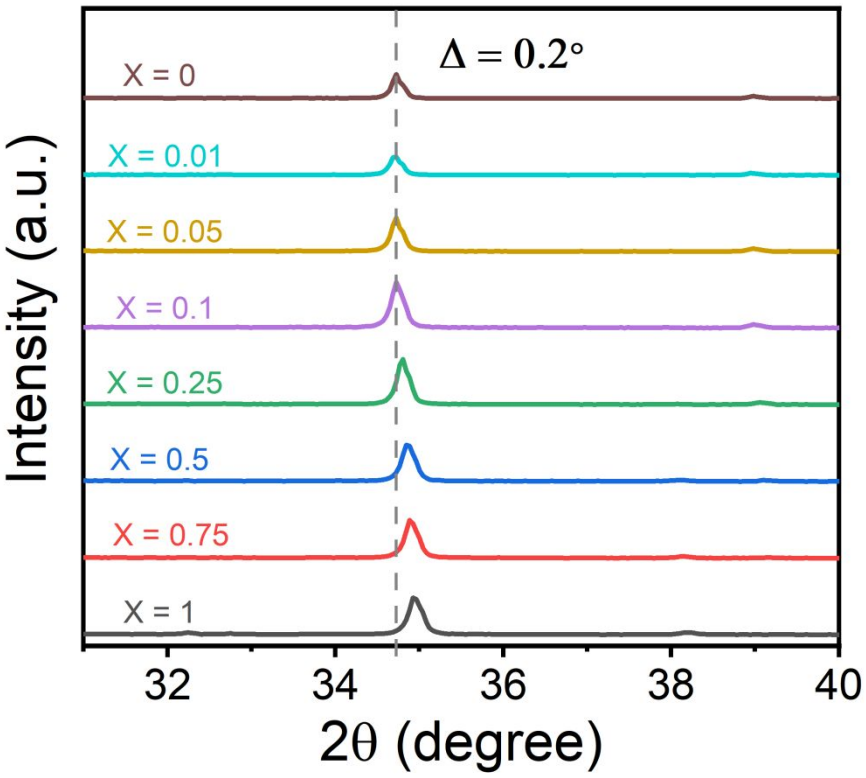

Figure S1. The (400) diffraction peaks of $Cs_2Ag_xNa_{1-x}FeCl_6$ (x = 0, 0.01, 0.05, 0.1, 0.25, 0.5, 0.75, and 1). With increasing Ag/(Ag+Na) ratio, The (400) diffraction peaks are almost unchanged from x = 0 to x = 0.1; these compositions exhibit a slightly monotonical shift of (400) diffraction peaks to higher 2θ values (~ 0.2°) from x = 0.1 to x = 1, related to the tiny lattice mismatch (0.6%) between $Cs_2NaFeCl_6$ (x = 0) and $Cs_2AgFeCl_6$ (x = 1).

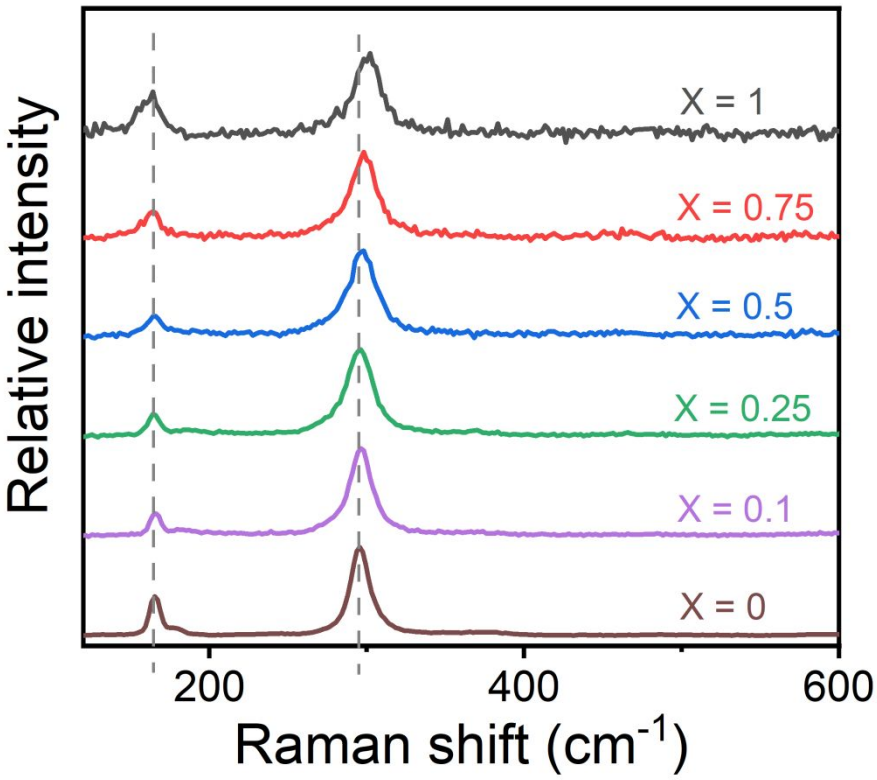

Figure S2. Raman spectra of $Cs_2Ag_xNa_{1-x}FeCl_6$ (x = 0, 0.1, 0.25, 0.5, 0.75, and 1).

According to previous studies,[1-3] for $Cs_2M'MX_6$ DPs (M' = Ag or Na; M = Bi or In; X = Cl or Br), the bonding strength of the M'-X (M' = Ag^+ or Na^+; X = Cl^- or Br^-) type bonds is found to be much stronger than that of the M-X (M = Bi^{3+} or In^{3+}) ones. Thus, the $[M'X_6]^{5-}$ (M' = Ag^+ or Na^+; X = Cl^- or Br^-) lattice vibrations dominate and the $[MX_6]^{3-}$ (M = Bi^{3+} or In^{3+}) Raman modes will turn silent. In other words, Raman spectroscopy of reported DPs only exhibit the lattice vibration signal of $[M'X_6]^{5-}$ (M' = Ag^+ or Na^+; X = Cl^- or Br^-) octahedron, but no Raman signal of $[MX_6]^{3-}$ (M = Bi^{3+} or In^{3+}) octahedron. However, for Fe-based DPs, bonding distortions will occur because of the large mismatch between $[FeCl_6]^{3-}$ and $[M'Cl_6]^{5-}$ (M' = Ag^+ or Na^+) sublattices, through strain relaxation, whereby the system must compensate by modifying bonding lengths. The bond length of Fe-Cl is shorter than that of M'-Cl (M' = Ag^+ or Na^+) (for $Cs_2NaFeCl_6$, Fe-Cl bond: 2.391 Å, Na-Cl bond: 2.773 Å; for $Cs_2AgFeCl_6$, Fe-Cl bond: 2.394 Å, Ag-Cl bond: 2.737 Å). The strain compensation of the Fe-Cl type bond cannot be ignored due to its relatively larger compression. Therefore, we anticipated that the Raman activity (lattice vibration signals) of $[FeCl_6]^{3-}$ and $[M'Cl_6]^{5-}$ (M' = Ag^+ or Na^+) are simultaneously observed by Raman spectroscopy in Fe-based DPs.

The Raman measurements are carried out using an inVia Raman Microscope spectrometer (Renishaw). The notable Raman active modes are located at 165 cm^{-1}, and between 295 and 302 cm^{-1}. With increasing Ag/(Ag+Na) ratio, the position of 165 cm^{-1} Raman peak has not changed and is independent of the Ag/Na ratio; but for the Raman peak of between 295 and 302 cm^{-1}, which is

related to the Ag/Na ratio and exhibit a slightly monotonical shift (~ 6.4 cm^{-1}). Moreover, we consider the Raman attribution of reported works in lead-free DPs and metal halide.[1-5] Therefore, it is reasonable that the Raman active modes of 165 cm^{-1}, and between 295 and 302 cm^{-1} are assigned to the lattice vibrations of $[FeCl_6]^{3-}$ and $[M'Cl_6]^{5-}$ (M' = Ag^+ or Na^+), respectively. The Raman activities of $[FeCl_6]^{3-}$ and $[M'Cl_6]^{5-}$ (M' = Ag^+ or Na^+) are simultaneously observed by Raman spectroscopy in lead-free DPs for the first time.

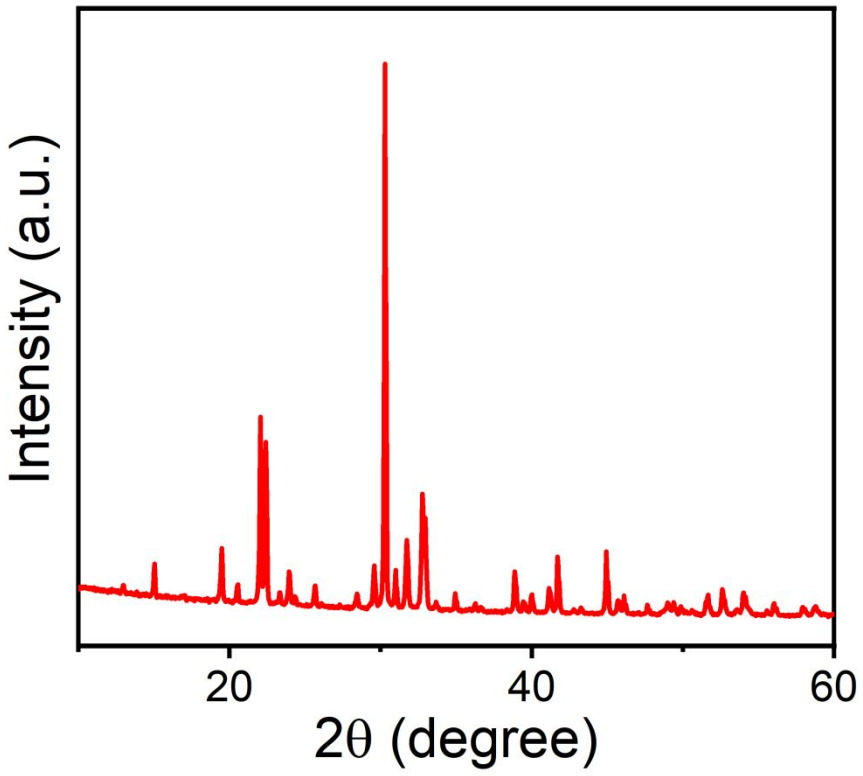

Figure S3. XRD pattern of $Cs_2FeCl_5(H_2O)$.

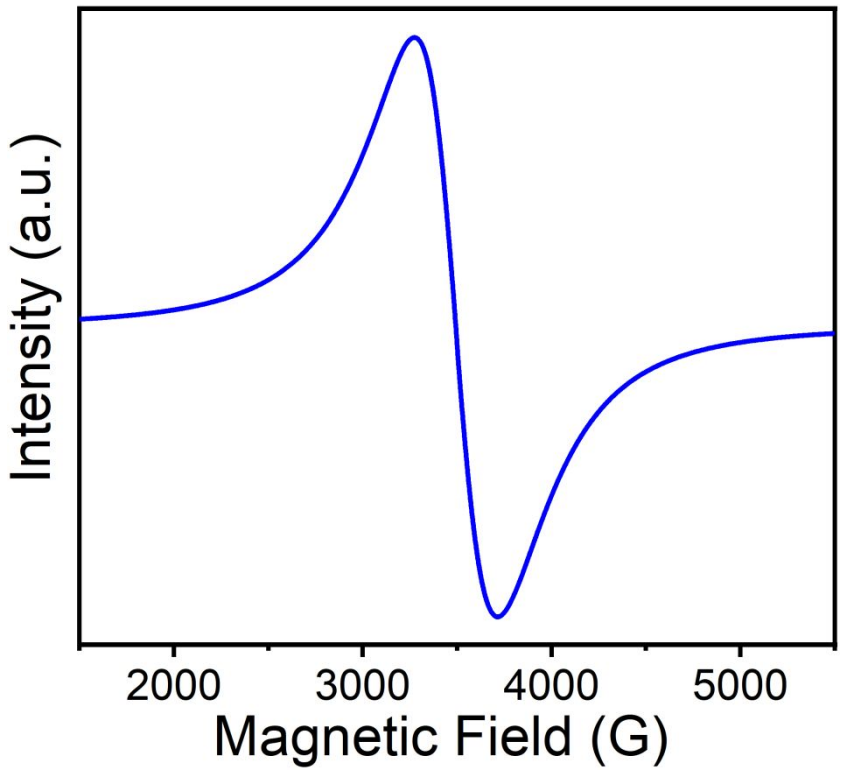

Figure S4. ESR signal of $Cs_2FeCl_5(H_2O)$.

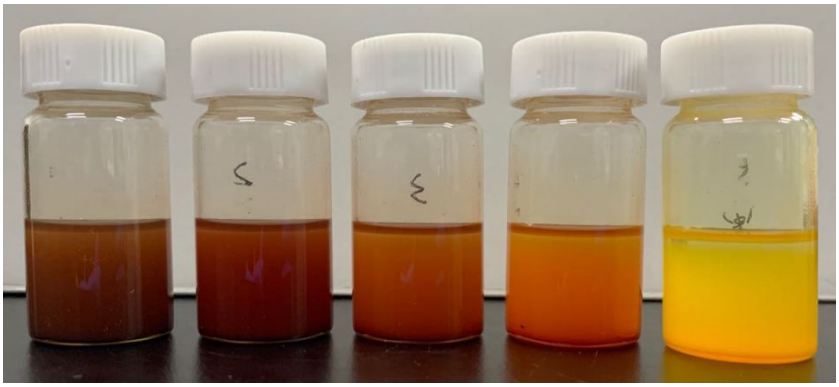

Figure S5. the photograph of as-synthesized $Cs_2Ag_xNa_{1-x}FeCl_6$ (x = 1, 0.75, 0.5, 0.25, and 0) colloidal NCs dispersed in mixed solution of 80% toluene and 20% isopropanol.

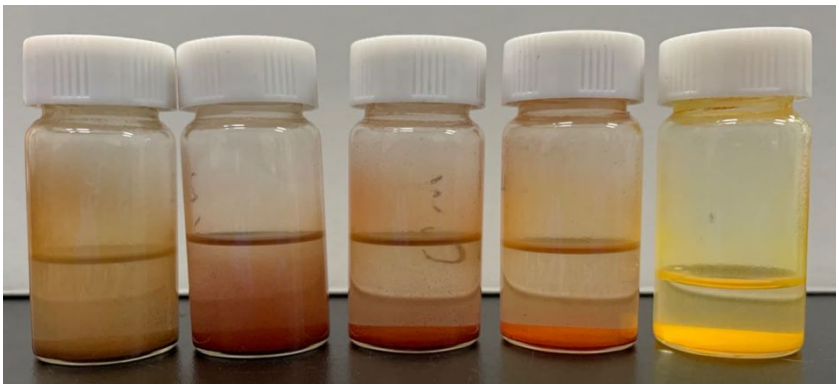

Figure S6. the photograph of as-synthesized $Cs_2Ag_xNa_{1-x}FeCl_6$ (x = 1, 0.75, 0.5, 0.25, and 0) colloidal NCs dispersed in hexane.

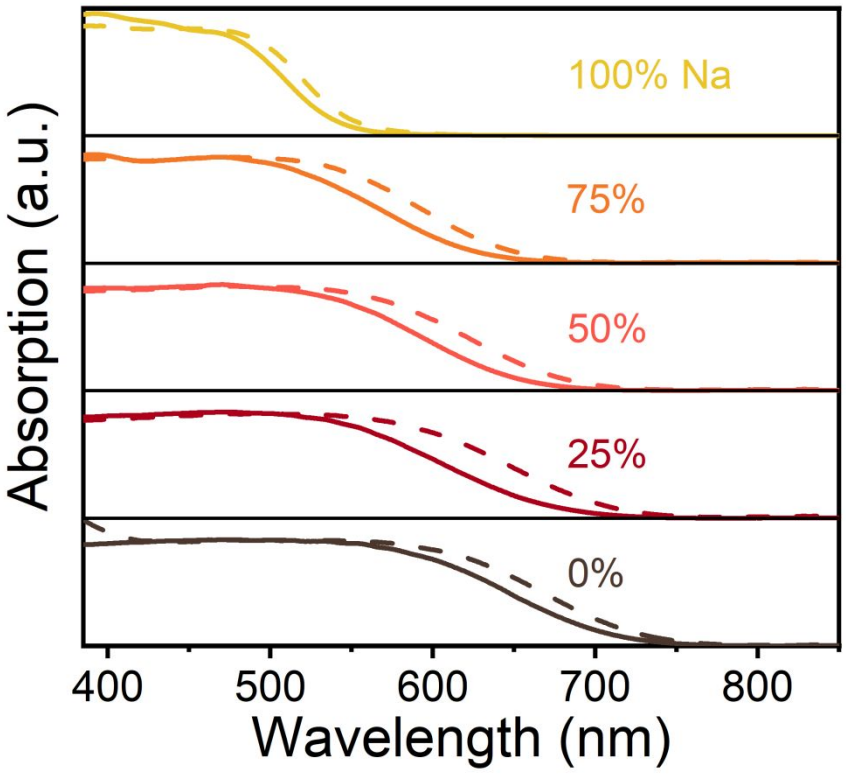

Figure S7. Steady-state absorption spectra of $Cs_2Ag_xNa_{1-x}FeCl_6$ (x = 0, 0.25, 0.5, 0.75, and 1) NCs precipitates (solid lines), compared to that of the corresponding SCs (dashed line).

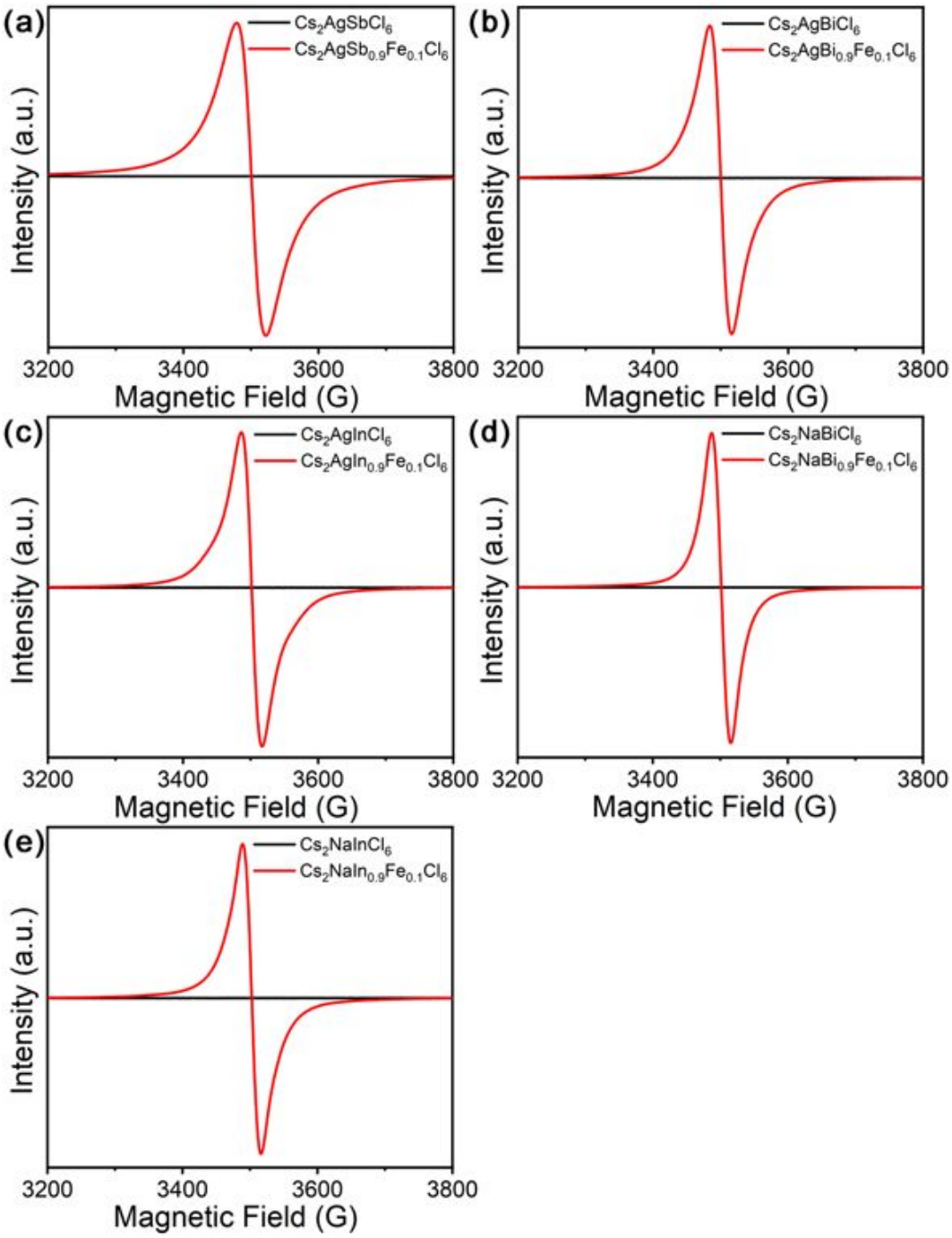

Figure S8. (a) ESR spectra of $Cs_2AgSbCl_6$ and $Cs_2AgSb_{0.9}Fe_{0.1}Cl_6$. (b) ESR spectra of $Cs_2AgBiCl_6$ and $Cs_2AgBi_{0.9}Fe_{0.1}Cl_6$. (c) ESR spectra of $Cs_2AgInCl_6$ and $Cs_2AgIn_{0.9}Fe_{0.1}Cl_6$. (d) ESR spectra of $Cs_2NaBiCl_6$ and $Cs_2NaBi_{0.9}Fe_{0.1}Cl_6$. (e) ESR spectra of $Cs_2NaInCl_6$ and $Cs_2NaIn_{0.9}Fe_{0.1}Cl_6$. (undoped DPs: black line; Fe-doped DPs: red line).

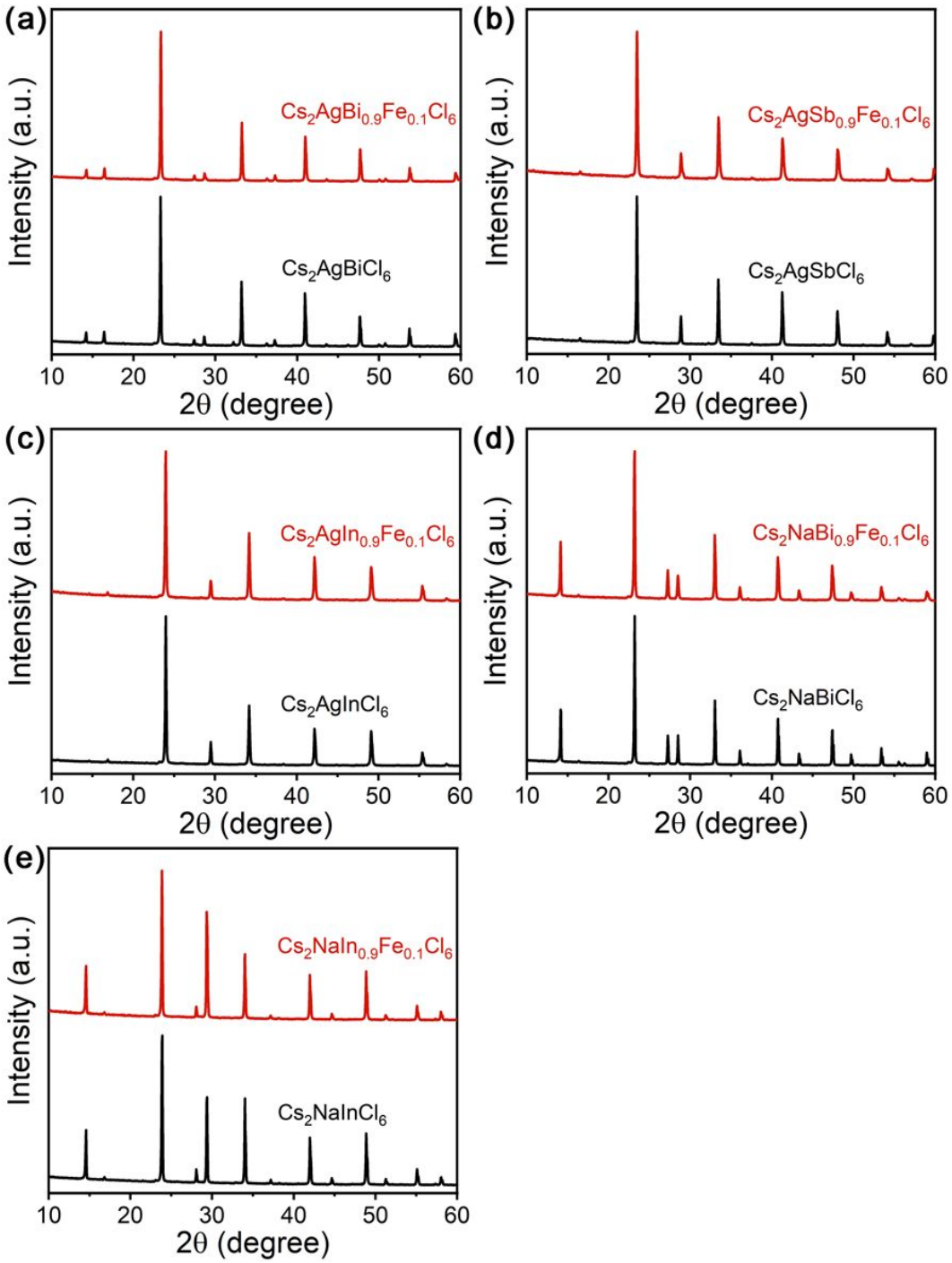

Figure S9. (a) XRD patterns of $Cs_2AgSbCl_6$ and $Cs_2AgSb_{0.9}Fe_{0.1}Cl_6$. (b) XRD patterns of $Cs_2AgBiCl_6$ and $Cs_2AgBi_{0.9}Fe_{0.1}Cl_6$. (c) XRD patterns of $Cs_2AgInCl_6$ and $Cs_2AgIn_{0.9}Fe_{0.1}Cl_6$. (d) XRD patterns of $Cs_2NaBiCl_6$ and $Cs_2NaBi_{0.9}Fe_{0.1}Cl_6$. (e) XRD patterns of $Cs_2NaInCl_6$ and $Cs_2NaIn_{0.9}Fe_{0.1}Cl_6$. (undoped DPs: black line; Fe-doped DPs: red line).

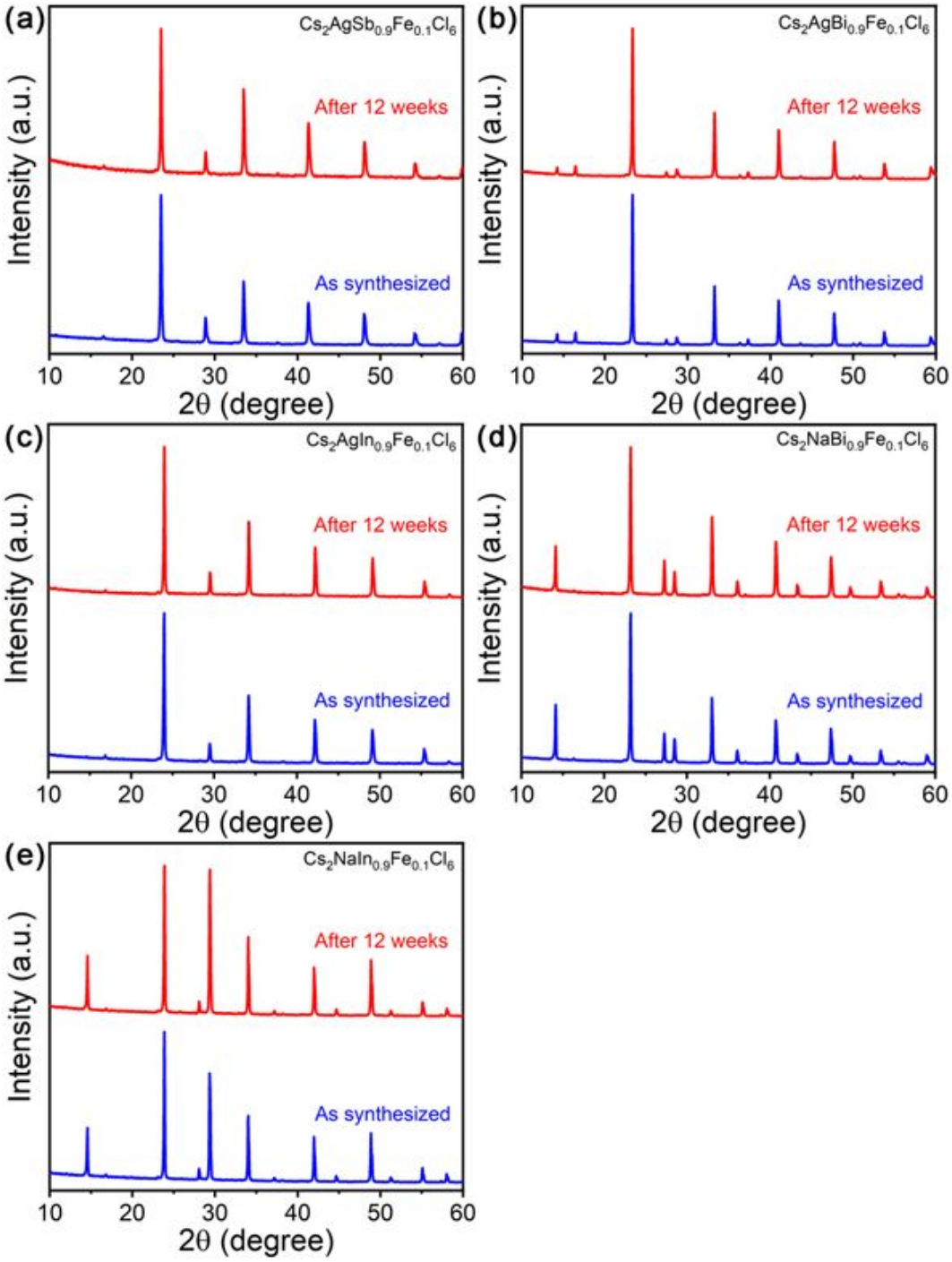

Figure S10. The air stability measurements of Fe-doped $Cs_2M'MCl_6$ (M' = Na or Ag; M = In, Sb or Bi), which stored in ambient air for 12 weeks. (a) $Cs_2AgSb_{0.9}Fe_{0.1}Cl_6$. (b) $Cs_2AgBi_{0.9}Fe_{0.1}Cl_6$. (c) $Cs_2AgIn_{0.9}Fe_{0.1}Cl_6$. (d) $Cs_2NaBi_{0.9}Fe_{0.1}Cl_6$. (e) $Cs_2NaIn_{0.9}Fe_{0.1}Cl_6$.

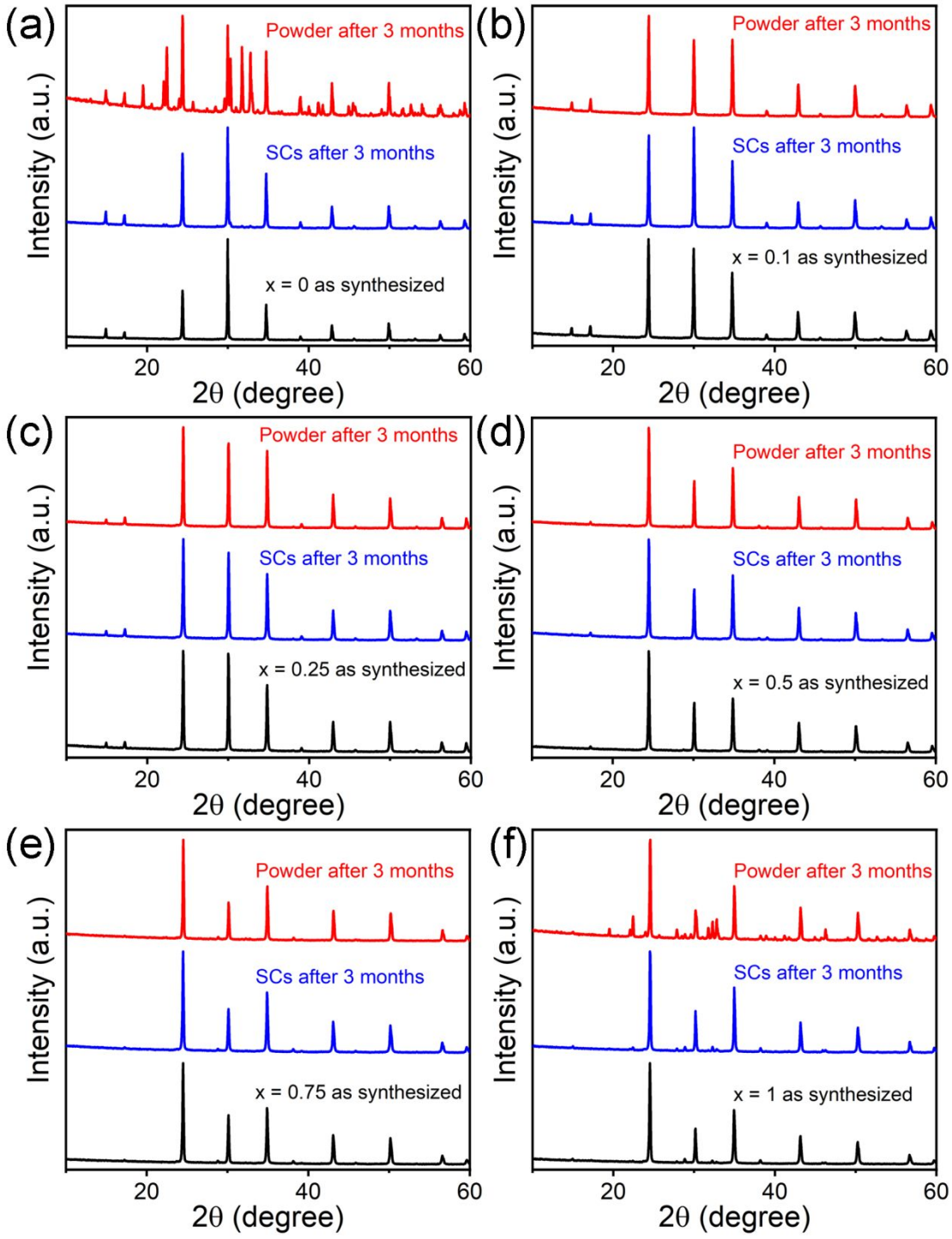

Figure S11. The air stability measurements of $Cs_2Ag_xNa_{1-x}FeCl_6$ (x = 0 (a), 0.1 (b), 0.25 (c), 0.5 (d), 0.75 (e), and 1 (f)) SCs and powders, which stored in ambient air for 3 months (black line: as synthesized samples; blue line: SCs; red line: powders). It is obvious that the air stability of alloying compositions ($0 < x < 1$) is better than that of pure compositions (x = 0 and 1), and the air stability of single crystals is better than that of powders.

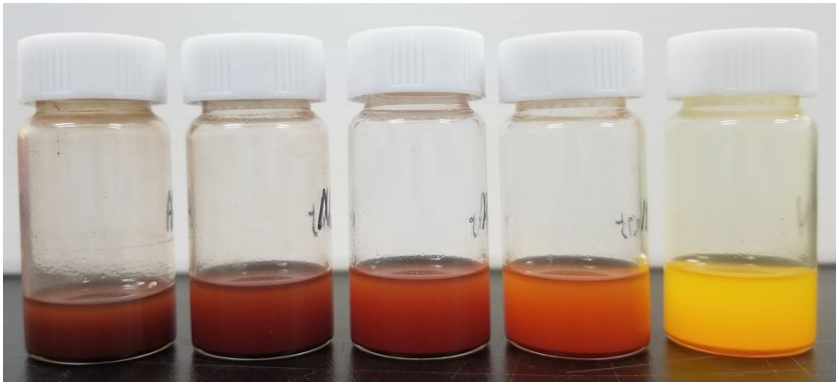

Figure S12. the photograph of $Cs_2Ag_xNa_{1-x}FeCl_6$ (x = 1, 0.75, 0.5, 0.25, and 0) colloidal NCs in mixed solution of 80% toluene and 20% isopropanol after exposed to the air for 2 weeks.

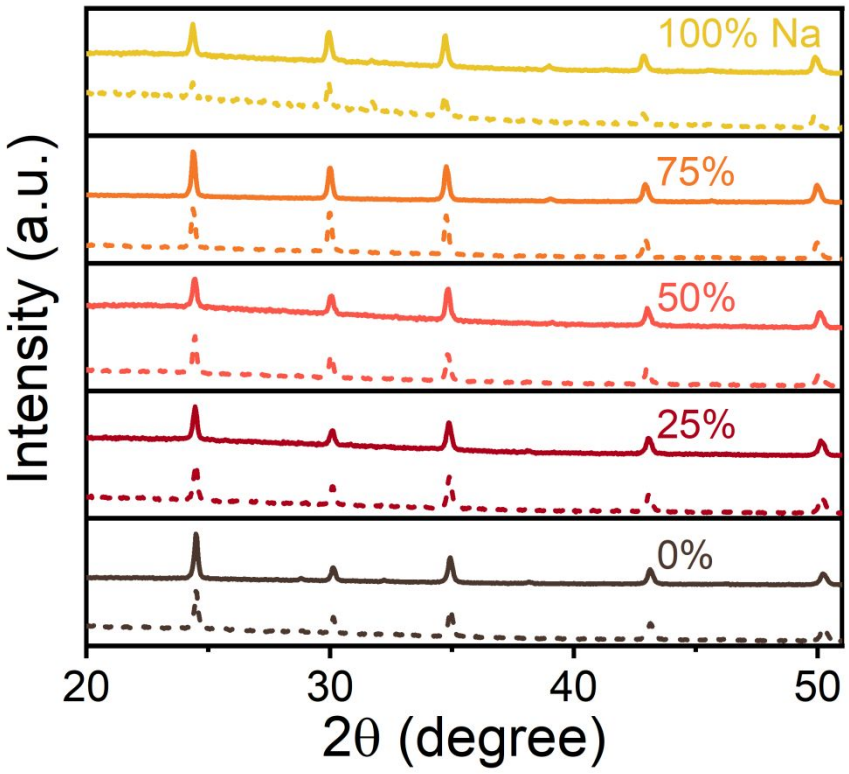

Figure S13. Normalized XRD patterns of $Cs_2Ag_xNa_{1-x}FeCl_6$ (x = 0, 0.25, 0.5, 0.75, and 1) colloidal NCs in mixed solution of 80% toluene and 20% isopropanol after stored in air for 2 weeks (solid lines), compared to corresponding as-synthesized samples (dashed line).

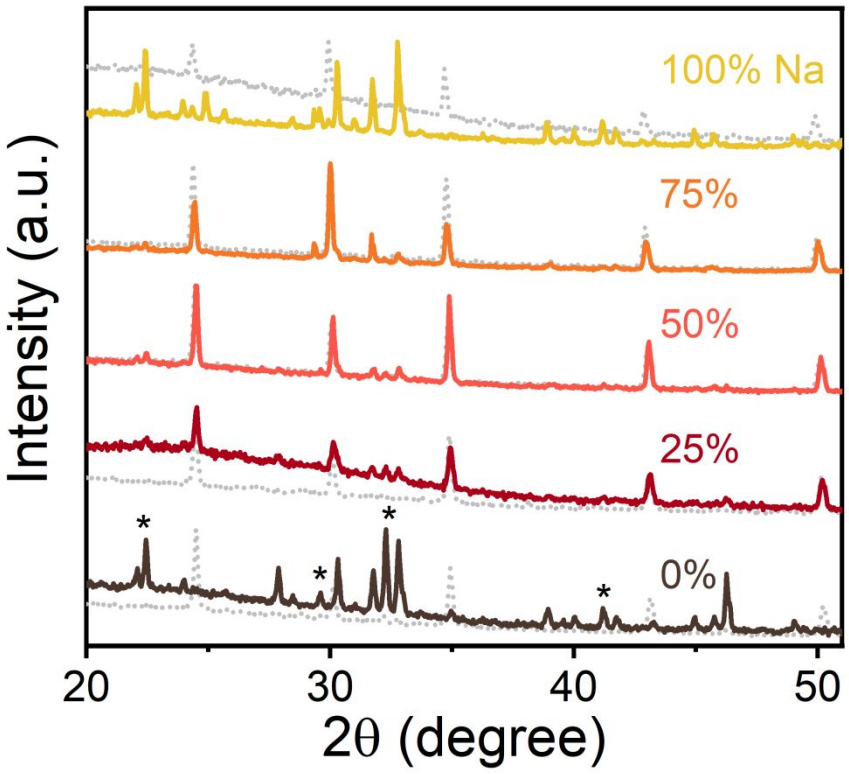

Figure S14. Normalized XRD patterns of $Cs_2Ag_xNa_{1-x}FeCl_6$ (x = 0, 0.25, 0.5, 0.75, and 1) NCs precipitates exposed to the air for less than 1h (solid lines), compared to corresponding as-synthesized samples (dashed line). The asterisks denote the impurity $Cs_2FeCl_5(H_2O)$ (**Figure S3**).

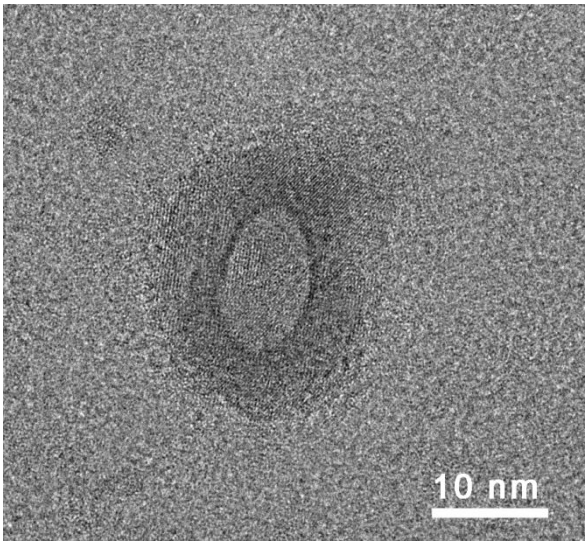

Figure S15. HRTEM image of single $Cs_2NaFeCl_6$ NC continuously exposed to electron beam about 30 seconds.

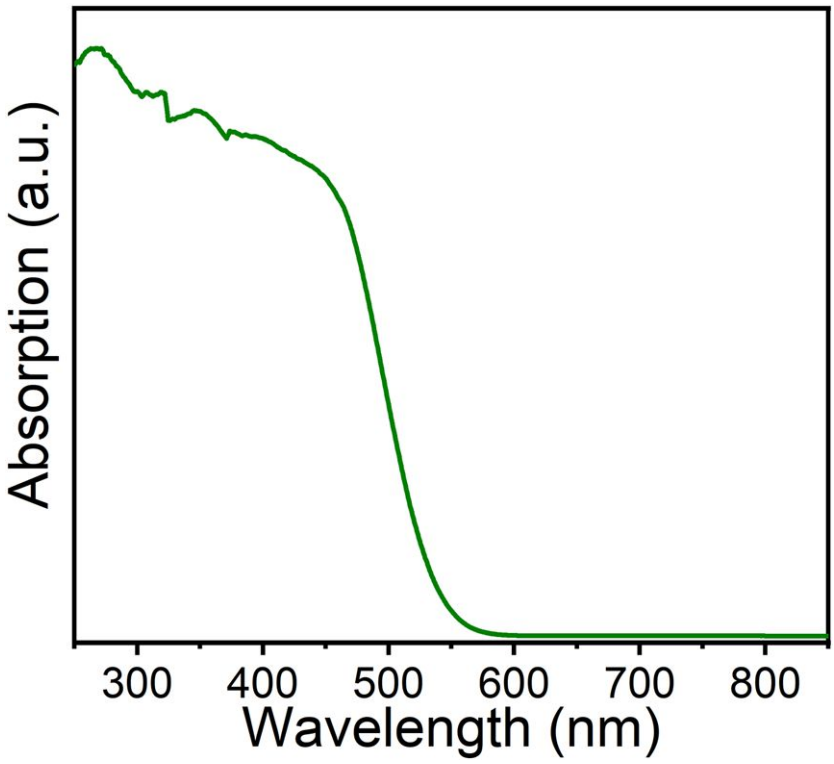

Figure S16. Steady-state absorption spectrum of $Cs_2FeCl_5(H_2O)$.

References

1 Steele, J. A.; Puech, P.; Keshavarz, M.; Yang, R.; Banerjee, S.; Debroye, E.; Kim, C. W.; Yuan, H.; Heo, N. H.; Vanacken, J.; et al. *ACS Nano*, **2018**, *12*, 8081-8090.

2 Han, P.; Mao, X.; Yang, S.; Zhang, F.; Yang, B.; Wei, D.; Deng, W.; Han, K. *Angew. Chem. Int. Ed.*, **2019**, *58*, 17231-17235.

3 Manna, D.; Kangsabanik, J.; Das, T. K.; Das, D.; Alam, A.; Yella, A. *J. Phys. Chem. Lett.*, **2020**, *11*, 2113-2120.

4 Marston, A. L.; Bush, S. F. *Appl. Spectrosc.*, **1972**, *26*, 579-584.

5 Kanno, H.; Hiraishi, J. *J. Raman Spectrosc.*, **1982**, *12*, 224-227.